

## Article

# Synthesis of Aragonite Whiskers by Co-Carbonation of Waste Magnesia Slag and Magnesium Sulfate: Enhancing Microstructure and Mechanical Properties of Portland Cement Paste

Junhao Ye <sup>1</sup>, Songhui Liu <sup>1,\*</sup> , Jingrui Fang <sup>2</sup>, Haibo Zhang <sup>1</sup>, Jianping Zhu <sup>1</sup> and Xuemao Guan <sup>1</sup>

<sup>1</sup> School of Materials Science and Engineering, Henan Polytechnic University, Jiaozuo 454003, China; 212106020022@home.hpu.edu.cn (J.Y.); zhzhhb@163.com (H.Z.); jianpingzhu@hpu.edu.cn (J.Z.); guanxuemao@hpu.edu.cn (X.G.)

<sup>2</sup> State Key Laboratory of Green Building Materials, China Building Materials Academy, Beijing 100024, China; fangjingrui@cbma.com.cn

\* Correspondence: liusonghui@hpu.edu.cn

**Abstract:** This study focused on the synthesis of aragonite whiskers through a synergistic wet carbonation technology utilizing waste magnesia slag (MS) and magnesium sulfate ( $\text{MgSO}_4$ ), aiming to improve the microstructure and mechanical properties of ordinary Portland cement (OPC) paste. The influence of  $\text{MgSO}_4$  concentration on the wet carbonation process, phase composition, and microstructure of MS was investigated. Furthermore, the effect of incorporating carbonated MS (C-MS) on the mechanical properties and microstructure of Portland cement paste was evaluated. Results showed that appropriate  $\text{MgSO}_4$  concentrations favored aragonite whisker formation. A concentration of 0.075 M  $\text{MgSO}_4$  yielded 86.6% aragonite with high aspect ratio nanofibers. Incorporating 5% of this C-MS into OPC increased the seven-day compressive strength by 37.5% compared to the control OPC paste. The improvement was attributed to accelerated hydration and reduced porosity by the filling effect and microfiber reinforcement of aragonite whiskers. MS demonstrated good  $\text{CO}_2$  sequestration capacity during carbonation. This study provides an effective method to synthesize aragonite whiskers from waste MS and use it to enhance cementitious materials while reducing  $\text{CO}_2$  emissions, which is valuable for the development of a sustainable cement industry.

**Keywords:** aragonite microfibers; wet carbonation; magnesium slag; magnesium sulfate; Portland cement



**Citation:** Ye, J.; Liu, S.; Fang, J.; Zhang, H.; Zhu, J.; Guan, X. Synthesis of Aragonite Whiskers by Co-Carbonation of Waste Magnesia Slag and Magnesium Sulfate: Enhancing Microstructure and Mechanical Properties of Portland Cement Paste. *Buildings* **2023**, *13*, 2888. <https://doi.org/10.3390/buildings13112888>

Academic Editor: Geo Paul

Received: 6 November 2023

Revised: 16 November 2023

Accepted: 17 November 2023

Published: 19 November 2023



**Copyright:** © 2023 by the authors. Licensee MDPI, Basel, Switzerland. This article is an open access article distributed under the terms and conditions of the Creative Commons Attribution (CC BY) license (<https://creativecommons.org/licenses/by/4.0/>).

## 1. Introduction

The cement industry is a major pillar supporting infrastructure development and construction activities worldwide [1–4]. However, cement production is also a significant contributor to global carbon dioxide ( $\text{CO}_2$ ) emissions, accounting for approximately 8–9% of total anthropogenic  $\text{CO}_2$  released into the atmosphere each year [5]. The calcination of limestone during clinker production and the combustion of fossil fuels in cement plants are the primary sources of the vast  $\text{CO}_2$  emissions. As the world's largest cement producer and consumer, China's cement industry emitted approximately 2.2 billion tons of  $\text{CO}_2$  in 2018, representing nearly 40% of global cement emissions [6]. The sheer scale of  $\text{CO}_2$  emissions from cement production poses a severe challenge to environmental sustainability and hinders the realization of carbon neutrality goals.

In light of the cement industry's disproportionately large carbon footprint, researchers worldwide have been prompted to develop and implement various solutions to curb emissions and achieve decarbonation of cement production [7–9]. The three main approaches are: (1) improving energy efficiency and shifting to renewable or low-carbon fuels like biomass [10]; (2) reducing clinker content by increasing supplementary cementitious materials (SCMs) [11–13]; and (3) applying carbon capture, utilization, and storage (CCUS)

technologies [14–17]. While switching to alternative fuels and optimizing energy can reduce CO<sub>2</sub> from fuel combustion, the calcination process inevitably releases CO<sub>2</sub> as an intrinsic byproduct. Hence, clinker substitution and CCUS present more direct approaches to tackle process emissions.

SCMs, like fly ash and slag, are established clinker replacements that improve the environmental profile of cement [18–20]. However, availability constraints and uneven distribution of such inorganic byproducts limit extensive substitution. On the other hand, CCUS offers a promising avenue for reducing process CO<sub>2</sub> emissions through permanent mineralization. This technique chemically binds the captured CO<sub>2</sub> into stable carbonates like calcium carbonate (CaCO<sub>3</sub>), enabling safe long-term storage [21]. Beyond sequestration, CCUS can also create value-added products with superior performance. The production of precipitated calcium carbonate (PCC) is a commercially established CCUS technology. Furthermore, research interest has expanded to the application of mineral carbonation for improving the properties of cementitious systems themselves while offsetting emissions [22].

The conversion of CO<sub>2</sub> into CaCO<sub>3</sub> during accelerated carbonation of cementitious materials not only sequesters CO<sub>2</sub> but also significantly alters its microstructural properties [23–25]. The formation of calcium carbonate provides nucleation sites for hydration products, reduces porosity, and acts as a filler to increase strength and durability [26,27]. However, the precipitation process of calcium carbonate is influenced by the environment and various ions, including CO<sub>3</sub><sup>2-</sup>, Ca<sup>2+</sup>, SO<sub>4</sub><sup>2-</sup>, Cl<sup>-</sup>, and Mg<sup>2+</sup> [28–30]. Among them, CO<sub>3</sub><sup>2-</sup> and Ca<sup>2+</sup> are the main participants in the carbonation reaction, and a high concentration of Ca<sup>2+</sup> and CO<sub>3</sub><sup>2-</sup> favors the precipitation process of calcium carbonate [31]. Therefore, some research has focused on increasing CO<sub>2</sub> concentration and enhancing the dissolution rate of Ca<sup>2+</sup> to accelerate the completion of the carbonation reaction [32]. In addition, an appropriate amount of Mg<sup>2+</sup> can alter the morphology and structure of calcium carbonate crystals, regulate their growth mode and appearance, and react with calcium carbonate and other components to form magnesium calcium carbonate [33]. However, a high concentration of Mg<sup>2+</sup> may inhibit the precipitation reaction of calcium carbonate, leading to a decrease in its formation. Shen et al. introduced MgCl<sub>2</sub> into the wet carbonation process of waste concrete powder and obtained calcium carbonate in the form of aragonite under a solution temperature of 80 °C [34]. Hu et al. investigated the formation of multi-crystalline calcium carbonate during the carbonation process of Portland cement in the presence of MgCl<sub>2</sub> using a thermodynamic model [35]. The results showed that although the proportion of aragonite increased with the initial concentration of magnesium chloride, the total amount of calcium carbonate gradually decreased. Furthermore, some studies have suggested that SO<sub>4</sub><sup>2-</sup> can retard the growth of calcium carbonate and affect the crystalline phase of calcium carbonate during the precipitation process [36].

On the other hand, Pidgeon method magnesium slag (MS) is an alkaline waste residue generated during the industrial magnesium refining process. As China is the largest producer of magnesium metal globally, MS reserves are abundant in the country. The composition of MS is primarily comprised of magnesium oxide (MgO) and other metal oxides (such as iron oxide, calcium oxide, etc.), with minimal variation between the components [37]. So far, MS has mainly been applied in areas such as filling cementitious materials and road-based materials [38–40]. However, due to the high proportion of magnesium oxide present in MS, it exhibits strong alkalinity and suffers from poor long-term stability. Therefore, the addition of modifying materials is typically necessary to ensure its usability. It is worth noting that magnesium oxide (MgO) can undergo a carbonation reaction with CO<sub>2</sub>. Meanwhile, the main mineral phase in MS is dicalcium silicate (C<sub>2</sub>S), which exhibits high carbonation activity. As a result, many researchers have studied and applied MS as a raw material for accelerated carbonation techniques. Liu et al. utilized a novel carbonation-hydration-curing method to enhance the hardening performance and microstructure of MS paste [41]. The results showed that a 2 h pre-carbonation effectively eliminated the instability of MS volume, and after 24 h of carbonation, the compressive

strength of MS blocks reached 90 MPa, with a CO<sub>2</sub> absorption capacity of 17.28%. Mo et al. used MS as a raw material and adopted accelerated carbonation to prepare calcium carbonate binders with a compressive strength of up to 119.5 MPa [42,43]. Furthermore, there have been reports indicating that MS can be used to produce aragonite through wet carbonation at room temperature [37]. These studies not only demonstrate the feasibility of MS in accelerated carbonation techniques but also reveal its potential as a precursor for preparing aragonite whiskers. The specialized needle-like morphology of the less common aragonite phase can provide substantial mechanical reinforcement. The fibrous nature of aragonite crystals substantially improves fracture toughness and prevents crack propagation in cementitious matrices. However, the effects of ionic species, like sulfates (SO<sub>4</sub><sup>2-</sup>) and magnesium (Mg<sup>2+</sup>), on the kinetics of aragonite formation during carbonation remain unclear.

Therefore, in this study, magnesium sulfate (MgSO<sub>4</sub>) was chosen as a crystal-modulating agent for calcium carbonate. By introducing Mg<sup>2+</sup> ions during the wet carbonation process of MS, the aim was to selectively control the crystal form of calcium carbonate and prepare materials rich in aragonite. X-ray diffraction (XRD), thermal analysis (TG-DTG), and scanning electron microscopy (SEM-EDS, NTS GmbH, Berlin, Germany) were used to investigate the influence of the coexistence of SO<sub>4</sub><sup>2-</sup> and Mg<sup>2+</sup> on the types of carbonation products, the microstructure of aragonite crystals, and nucleation and growth. Additionally, the ability of aragonite whiskers synthesized from MS to sequester CO<sub>2</sub> was evaluated. Finally, C-MS with suitable concentrations was added to ordinary Portland cement (OPC) at different substitution levels to study its effects on the mechanical properties and microstructure of the cementitious material. This study not only explores the influence of the coexistence of SO<sub>4</sub><sup>2-</sup> and Mg<sup>2+</sup> on the morphology of calcium carbonate crystals but also develops a novel magnesium slag-based microfiber material that enhances the mechanical properties of cement while reducing carbon emissions.

## 2. Experimental Design

### 2.1. Raw Materials

In this study, the Pidgeon method magnesium slag (MS) used was obtained from Yulin City, Shaanxi Province, China. The ordinary Portland cement (OPC) was provided by the China Building Materials Academy. Chemical composition analysis of MS and OPC was conducted using an ARL-9800XP X-ray fluorescence spectrometer (XRF), and the specific results are presented in Table 1. The CO<sub>2</sub> gas used in the wet carbonation process had a concentration of 99.9% and was purchased from a gas supplier. Deionized water was prepared in the laboratory. For this study, analytical reagent-grade magnesium sulfate (MgSO<sub>4</sub>) was purchased from Shanghai Aladdin Bio-Chem Technology Co., Ltd., Shanghai, China, and used as a crystal-modulating agent for calcium carbonate in the wet carbonation process of MS.

**Table 1.** Chemical composition of the raw materials (in wt.%).

Oxide	SiO <sub>2</sub>	Al <sub>2</sub> O <sub>3</sub>	CaO	Fe <sub>2</sub> O <sub>3</sub>	MgO	Others
MS	29.88	1.06	50.98	3.52	11.27	3.29
OPC	23.17	5.37	61.86	3.32	2.78	3.5

Before the experiment, MS was dried at 105 °C until a constant weight was achieved and then milled using a ball mill. The particle size distribution of the MS powder was analyzed using a Malvern Mastersizer 3000E laser diffraction analyzer, and the specific results are shown in Figure 1. In addition, X-ray diffraction (XRD) analysis of the powder was conducted using a Smart Lab Rigaku X-ray diffractometer to determine the mineral phase composition, as detailed in Figure 2. The main crystal phases identified in MS were dicalcium silicate (C<sub>2</sub>S), calcium hydroxide (CH), brucite (Mg(OH)<sub>2</sub>, MH), and MgO.

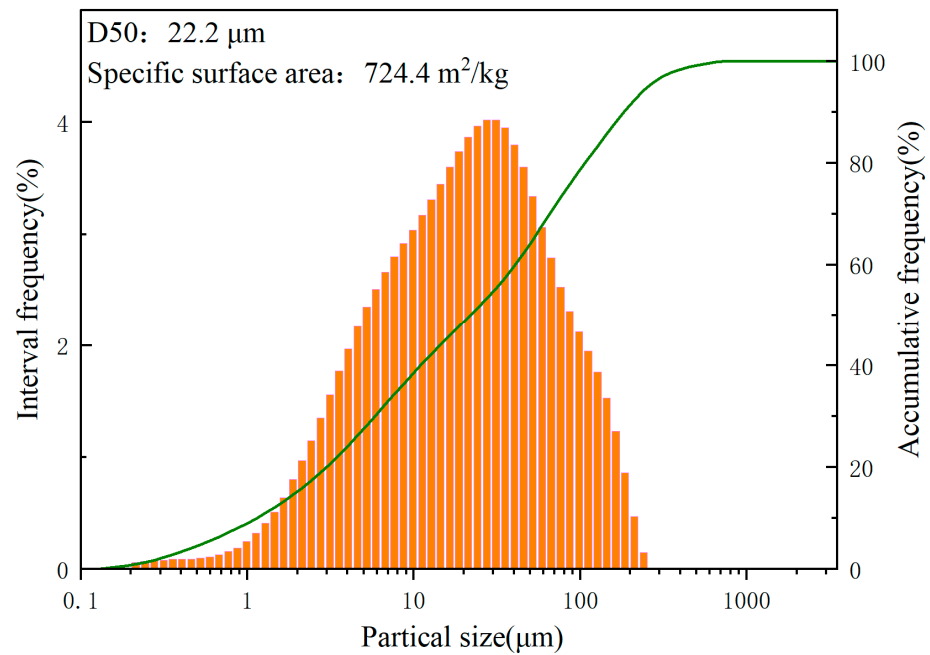


**Figure 1.** The particle sizes of MS.

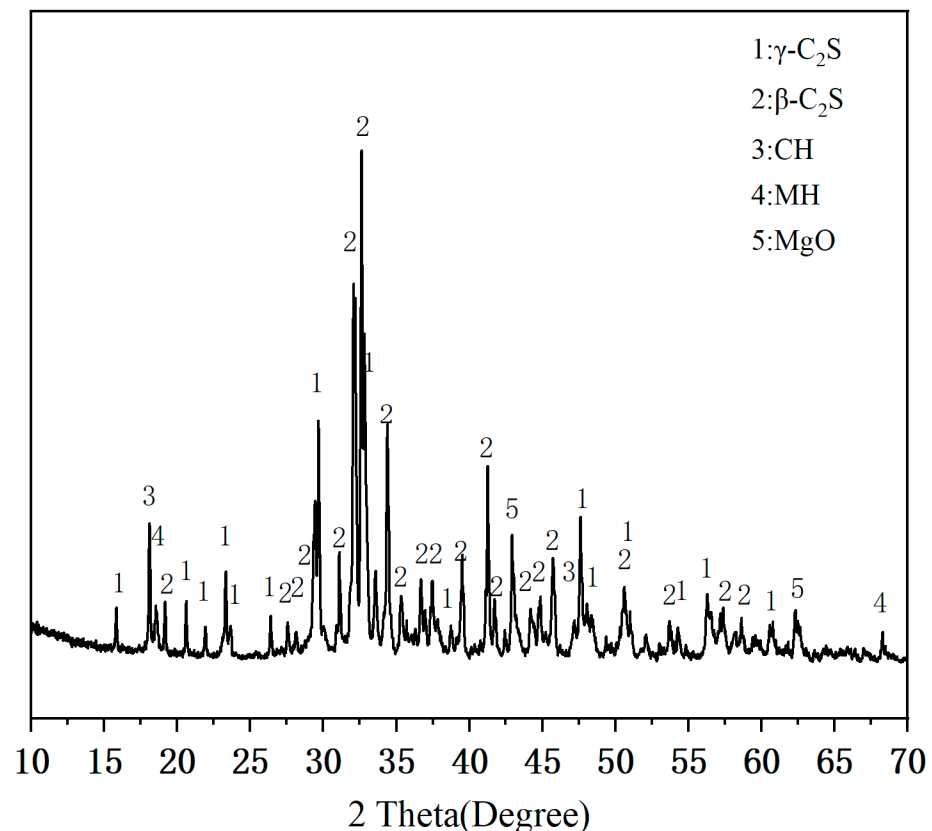


**Figure 2.** X-ray diffraction patterns of MS.

### 2.2. Preparation of C-MS and Curing of Cement Samples

The experimental procedure in this study is illustrated in Figure 3. Firstly, magnesium sulfate ( $\text{MgSO}_4$ ) solutions of various concentrations (0.01 mol/L, 0.03 mol/L, 0.05 mol/L, 0.075 mol/L, 0.1 mol/L, 0.2 mol/L, 0.3 mol/L, 0.4 mol/L, and 0.5 mol/L) were prepared by dissolving  $\text{MgSO}_4$  in deionized water. The MS powder was then mixed with the

magnesium sulfate solution at a ratio of 1/40 by magnetic stirring. The apparatus was heated to 80 °C with a stirring rate set at 400 r/min. Throughout the experiment, plastic wrap was used to cover the apparatus to prevent moisture evaporation at high temperatures. After 10 min of stirring, carbonation was initiated by introducing high-concentration CO<sub>2</sub> at a ventilation rate of 0.1 L/min/5 g MS using an aeration device. The carbonation reaction lasted for 120 min. Upon completion of carbonation, the suspension was filtered, and the resulting carbonated MS samples (C-MS) were collected and repeatedly washed with ethanol, followed by placement in a vacuum drying chamber at 50 °C.

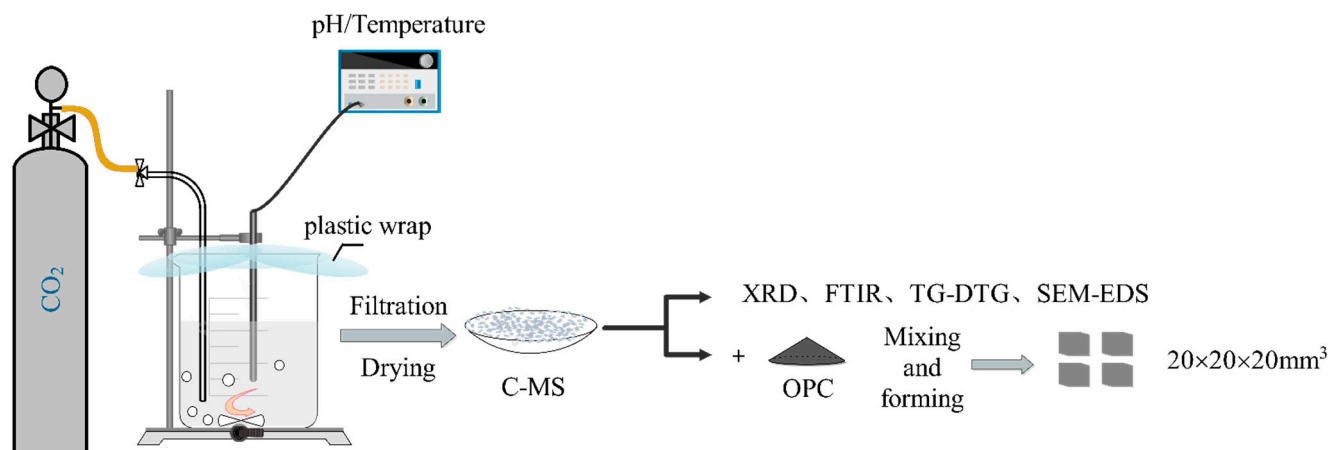


**Figure 3.** Experimental procedure.

Next, the samples were ground using an agate mortar and subjected to X-ray diffraction (XRD), thermal analysis (TG-DTG), Fourier transform infrared spectroscopy (FTIR), and scanning electron microscopy–energy-dispersive spectroscopy (SEM–EDS) testing. It is important to note that S-0 represents the MS sample carbonated for 120 min in pure water at 80 °C, while S-0.01 and so on represent the corresponding MS samples carbonated for 120 min at the respective magnesium sulfate concentrations.

To evaluate the impact of C-MS on the mechanical properties of cement paste, C-MS was partially substituted for ordinary Portland cement (OPC) at mass fractions of 0–5%. The water-to-cement ratio was set at 0.4. Cubic molds with dimensions of 20 mm were selected, and the cement paste was thoroughly mixed before being poured into the molds. The curing conditions were maintained at an environmental temperature of  $24 \pm 1$  °C and relative humidity (RH) exceeding 95%.

After 24 h of curing, the samples were de-molded, and three specimens from each group were subjected to compressive strength testing three times to obtain the average compressive strength values. The remaining specimens were further cured in saturated lime water at  $20 \pm 1$  °C. Compressive strength tests were conducted at 3, 7, and 28 days.

### 2.3. Test Methods

#### 2.3.1. pH Changes

The pH value of the MS suspension was monitored in real time using a precision digital pH meter (REX PHS-3C model) [37]. Before injecting CO<sub>2</sub> into the system, the pH data-recording interval was set to every 30 s. This was done to promptly record the initial pH value of the suspension before the reaction started and observe the changes that occurred over time. Once CO<sub>2</sub> injection commenced, the pH data-recording interval was extended to every minute to better cope with the increased reaction rate and the intensity of pH fluctuations.

### 2.3.2. X-ray Diffraction Analysis (XRD)

XRD analysis was performed using a Smart Lab model Rigaku X-ray diffractometer manufactured in Akishima City, Tokyo, Japan, with Cu K $\alpha$  radiation and operating at a voltage of 40 kV and current of 150 mA [14]. To control the scanning rate, it was set to 10°/min. The angle range in this experiment was from 5° to 70° (2 $\theta$ ). In order to quantify the mineral content in the sample, the XRD results were analyzed by Rietveld full spectrum fitting semi-quantitative analysis.

### 2.3.3. Thermal Analysis (TG-DTG)

The thermal analysis experiments in this study were conducted using a differential thermal balance (model BJ-HCT-3) manufactured in Beijing, China [11]. Before thermal analysis, 15  $\pm$  1 mg of dried C-MS powder was prepared and placed in a crucible. The purpose was to determine the relationship between sample mass loss and temperature variation. The temperature range was set from 40 °C to 1000 °C, with a heating rate of 10 °C/min, to maintain consistent conditions throughout the analysis.

### 2.3.4. Fournier Transform Infrared Analysis (FTIR)

To observe and analyze the functional groups, chemical bonds, and other relevant infrared-active features in the samples, FT-IR (Fourier Transform Infrared) testing was conducted using the PerkinElmer Frontier infrared spectrometer. The testing range was set at 400–4000 cm<sup>-1</sup>, and a resolution of 4 cm<sup>-1</sup> was selected. This ensured the ability to accurately capture subtle frequency changes and provide a better interpretation of the chemical composition of the samples.

### 2.3.5. Scanning Electron Microscopy Analysis (SEM)

SEM (Scanning Electron Microscopy) technology was used to observe the microstructural changes of the samples at different concentrations of magnesium sulfate to study the growth characteristics of aragonite size. In addition, the fracture surface of the cement paste was observed and analyzed. The SEM used in this study was the Merlin Compact produced by NTS GmbH, Berlin, Germany. The equipment worked in high vacuum mode during testing and an acceleration voltage of 15 kV was set to obtain high-quality images. To ensure the accuracy and reliability of the test results, the samples were treated with a gold spray before testing to improve the samples' conductivity and obtain clearer images.

## 3. Results and Discussion

### 3.1. pH Monitoring during MS Carbonation

The pH dynamics of MS suspension during the wet carbonation process in real-time were investigated. Figure 4 presents the pH curves of MS in pure water and MgSO<sub>4</sub> solution. The pH variation of the MS suspension can be divided into three stages.

Initially, in the pre-injection stage before CO<sub>2</sub> injection (0–10 min), the pH value slightly increases, but the increase is minimal. This is because alkaline ions in the MS start to dissolve before CO<sub>2</sub> is introduced, leading to a slight pH increase in the suspension. Subsequently, after the injection of CO<sub>2</sub> gas, the pH value of the suspension rapidly decreases within ten minutes. This is due to the dissolved CO<sub>2</sub> gas forming carbonic acid in the aqueous solution, which then reacts with dissolved Ca<sup>2+</sup> to precipitate, resulting in a pH decrease. During this stage, the precipitation reaction of calcium carbonate and the dissolution of alkaline ions occur simultaneously. However, the precipitation reaction is faster and consumes a significant number of alkaline ions in the suspension, causing a sharp pH drop. After approximately 20 min, the pH value approaches neutrality and stabilizes, indicating that the carbonation reaction of MS is nearing saturation.

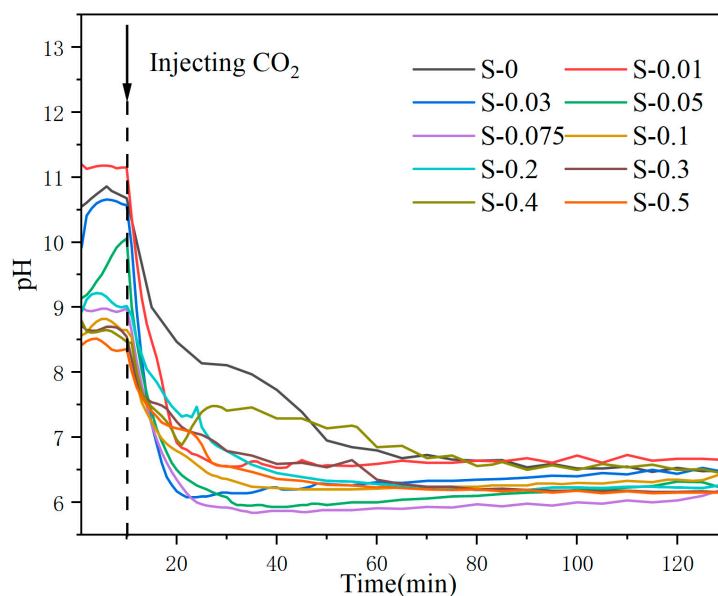


**Figure 4.** The pH curves of MS.

It is noteworthy that the concentration of magnesium sulfate significantly affects the rate of pH decrease. When the concentration of magnesium sulfate is below 0.1 M, the rate of pH decrease increases with the increase in magnesium sulfate concentration. However, when the concentration exceeds 0.1 M, the pH curve exhibits a slight upward trend after the decrease, and the final stable pH is noticeably higher than that of the groups with concentrations below 0.1 M. Additionally, it can be observed that it takes 40 min for MS to reach a stable pH in pure water, while this time is halved in the presence of magnesium sulfate solution, indicating that the presence of  $\text{MgSO}_4$  significantly accelerates the carbonation reaction of MS. This can be primarily attributed to the co-ion effect, in which the dissolved  $\text{Mg}^{2+}$  interacts with  $\text{Ca}^{2+}$  ions, altering the precipitation reaction rate [44].

### 3.2. Characterization of MS Carbonation Products

#### 3.2.1. Phase Compositions of Carbonated MS

The XRD analysis results of C-MS samples in pure water and different concentrations of  $\text{MgSO}_4$  solution are shown in Figure 5. The semi-quantitative analysis results are listed in Table 2.

According to the experimental results, during the wet carbonation reaction in pure water, MS generates two crystalline forms of calcium carbonate, namely calcite and aragonite. Among them, aragonite accounts for 47.9% of the total yield. When  $\text{MgSO}_4$  solution is used as the carbonation medium, the yield of aragonite shows an increasing trend. At a concentration of 0.03 M, the content of aragonite increases to 76.1%, becoming the main phase.

With further increase in  $\text{MgSO}_4$  concentration, the content of aragonite continues to increase. However, when the  $\text{MgSO}_4$  concentration reaches 0.1 M, the diffraction peaks of calcite completely disappear, and a new phase, gypsum ( $\text{CaSO}_4 \cdot 2\text{H}_2\text{O}$ ), appears [45–47]. The content of gypsum gradually increases with the increase in  $\text{MgSO}_4$  concentration, reaching 35.1% at 0.5 M.

This indicates that the addition of  $\text{Mg}^{2+}$  can stabilize the crystal structure of aragonite, inhibit its transformation to calcite, and significantly increase the yield of aragonite. However, when the  $\text{MgSO}_4$  concentration in the suspension reaches a certain level, part of the  $\text{Ca}^{2+}$  forms calcium carbonate with aragonite crystal under the action of  $\text{Mg}^{2+}$ , while the remaining  $\text{Ca}^{2+}$  combines with  $\text{SO}_4^{2-}$  to form gypsum, resulting in the complete disappearance of the calcite phase.

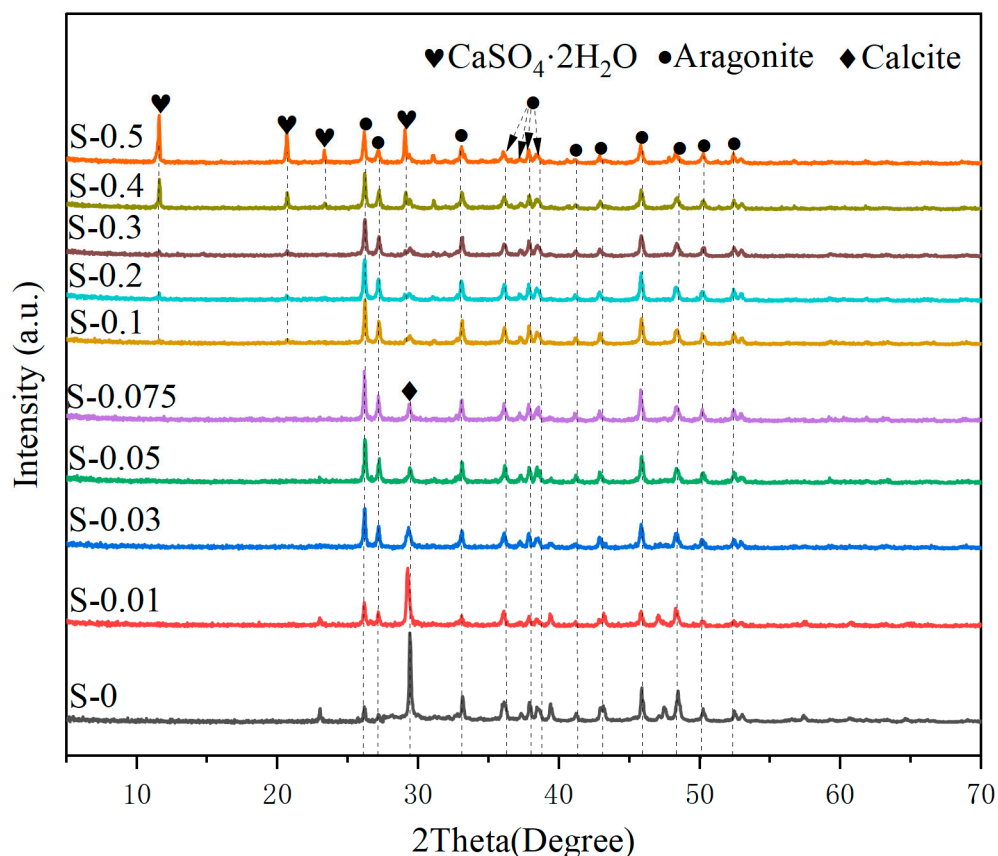


Figure 5. The XRD analysis results of C-MS.

Table 2. The semi-quantitative analysis results.

Concentration (mol/L)	Calcite (%)	Aragonite (%)	CaSO <sub>4</sub> ·2H <sub>2</sub> O (%)
0	52.1%	47.9%	0
0.01	55%	45%	0
0.03	23.9%	76.1%	0
0.05	14.4%	85.6%	0
0.075	15.4%	84.6%	0
0.1	0	95.8%	4.2%
0.2	0	94.2%	5.8%
0.3	0	94.6%	5.4%
0.4	0	77.7%	22.3%
0.5	0	64.9%	35.1%

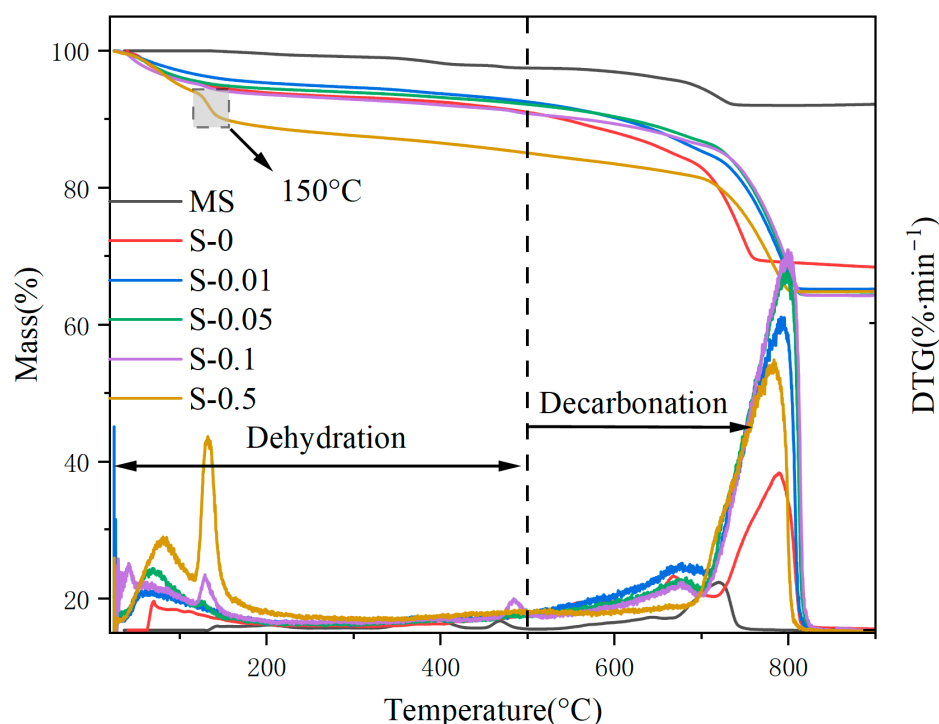
Table 3 provides a comparison of aragonite content prepared from different raw materials. Previous studies have mostly focused on using MgCl<sub>2</sub> as an aragonite crystal stabilizer. Shen et al. conducted carbonation experiments on recycled concrete powder at a concentration of 0.4 M MgCl<sub>2</sub> for 120 min, successfully synthesizing well-formed aragonite crystals, but with an aragonite content of only 41.34% [34]. Similarly, when cement was used as the raw material and carbonation was conducted at 0.05 M MgCl<sub>2</sub> for 120 min, the aragonite content was only 62.47% [48]. In contrast, in this study, using a concentration of 0.05 M MgSO<sub>4</sub>, the aragonite content reached 86.6%. These results further demonstrate that using MS as the raw material and MgSO<sub>4</sub> for controlling calcium carbonate crystals, the aragonite content obtained is superior to that achieved using cement and recycled concrete powder.

**Table 3.** Comparison of aragonite content prepared from different raw materials.

Materials	Crystal Modifier	Concentration /M	Temperature /°C	Time/min	Aragonite/wt%	Reference
Fine recycled concrete waste	MgCl <sub>2</sub>	0.4	80	120	41.34	[34]
Cement	MgCl <sub>2</sub>	0.05	80	120	62.47	[48]
MS	MgSO <sub>4</sub>	0.05	80	120	85.6	This work

### 3.2.2. Thermal Analysis

Figure 6 displays the TG-DTG curves of C-MS samples at different MgSO<sub>4</sub> concentrations. To illustrate the phase transformation behavior clearly, only the results of 0, 0.01, 0.05, 0.1, and 0.5 M concentrations are shown. From the curves, two weight loss intervals can be observed: 50–500 °C and 500–800 °C, corresponding to the dehydration of gel and hydration products and the thermal decomposition of calcium carbonate, respectively [49,50].

**Figure 6.** The TG-DTG curves of C-MS.

The DTG curve of MS clearly shows the thermal decomposition peak of calcium carbonate, indicating that the raw material MS has undergone a slight carbonation reaction with atmospheric CO<sub>2</sub> during transportation, leading to the formation of calcium carbonate. Furthermore, compared to the control group S-0, the DTG curves of the experimental groups show an obvious increase in the peak intensity of aragonite decomposition between 700 and 800 °C with the increase in MgSO<sub>4</sub> concentration. When the MgSO<sub>4</sub> concentration reaches 0.1 M, the DTG curve of the experimental group S-0.1 exhibits a dehydration weight loss peak of CaSO<sub>4</sub>·2H<sub>2</sub>O at 150 °C, with the highest peak intensity observed at 0.5 M [51–53]. This indicates that when the MgSO<sub>4</sub> concentration is below 0.1 M, the carbonation products of MS mainly consist of calcium carbonate and gel, while when the MgSO<sub>4</sub> concentration exceeds 0.1 M, a new phase, CaSO<sub>4</sub>·2H<sub>2</sub>O, appears in the products, and the peak intensity increases with the MgSO<sub>4</sub> concentration.

In addition, the fixed carbon contents of the experimental groups S-0, S-0.01, S-0.05, S-0.1, and S-0.5 were calculated to be 24.5%, 30.4%, 31.14%, 29.66%, and 22.27%, respectively. It can be observed that the fixed carbon content decreases at a concentration of

0.1 M, which is attributed to the formation of dihydrate gypsum, causing the consumption of part of the  $\text{Ca}^{2+}$  and ultimately resulting in a decrease in the total amount of calcium carbonate generated.

### 3.2.3. Evolution of the Siliceous Phase

To investigate the evolution of the siliceous phase in MS, this study analyzed C-MS samples in pure water and solutions with different concentrations of  $\text{MgSO}_4$  using FTIR testing. The test results are shown in Figure 7.

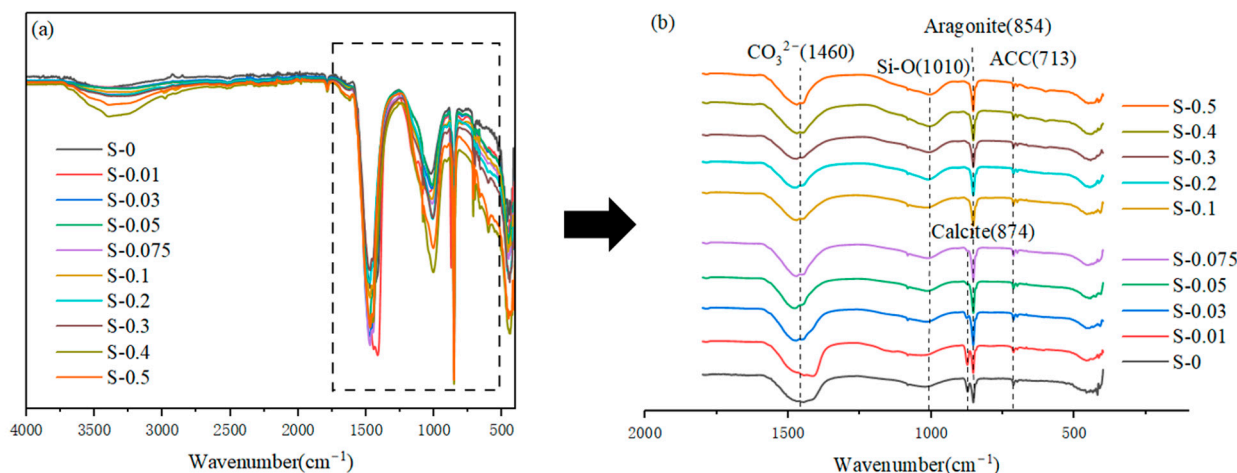


**Figure 7.** The test results of C-MS, (a) 400–4000  $\text{cm}^{-1}$ , (b) 100–2000  $\text{cm}^{-1}$ .

According to the results in Figure 7b, peaks corresponding to the out-of-plane bending vibration ( $\nu^4$ ) and asymmetric stretching vibration ( $\nu^3$ ) are observed at 854  $\text{cm}^{-1}$  and 1460  $\text{cm}^{-1}$ , respectively. Particularly, in the S-0 experimental group, the vibrational peaks of aragonite are visible, further confirming that aragonite can be generated in MS through wet carbonation in a pure water environment. As the  $\text{MgSO}_4$  concentration increases, the intensity of the aragonite vibrational peaks also increases.

It should be noted that only in the S-0, S-0.01, S-0.03, and S-0.05 experimental groups, the peak at 874  $\text{cm}^{-1}$  represents the  $\nu^2$  vibration of the S-O bond, indicating the presence of calcite. However, as the  $\text{MgSO}_4$  concentration increases, the intensity of this peak gradually weakens until it completely disappears in the S-0.075 experimental group. This indicates that when the  $\text{MgSO}_4$  concentration is below 0.075 M, both aragonite and calcite crystalline forms coexist in the generated calcium carbonate. Once the concentration exceeds this range, the calcite vibrational peak disappears, and a vibrational peak corresponding to dihydrate gypsum appears at 3300  $\text{cm}^{-1}$  [54]. The intensity of this peak increases with the  $\text{MgSO}_4$  concentration, while calcite becomes the dominant crystalline phase of calcium carbonate, which is consistent with the results shown in Table 2.

According to the results in Figure 7b, it can be observed that the intensity of the Si-O bond vibration peak does not increase with the concentration of magnesium sulfate solution when it is below 0.075 M. However, when the solution concentration exceeds 0.1 M, the intensity of the Si-O bond vibration peak increases with the concentration of magnesium sulfate solution. This phenomenon indicates an enhancement in the aggregation degree of silica gel. Furthermore, the peaks located at 1010  $\text{cm}^{-1}$  and 713  $\text{cm}^{-1}$  represent the stretching vibrations of Si-O in the gel and amorphous calcium carbonate (ACC), respectively, further demonstrating that gel and ACC are also formed in MS after carbonation. Based on the research findings, it can be observed that in the MS wet carbonation reaction, when using magnesium sulfate solution as the solvent medium at 80  $^\circ\text{C}$ , the crystalline phase of the generated calcium carbonate undergoes changes with increasing solution concentration. In addition to aragonite becoming the dominant crystalline phase, an increase in

degree of polymerization of silica gel is also observed when the magnesium sulfate solution concentration exceeds 0.1 M.

### 3.2.4. Microstructure

Figure 8 illustrates the morphological evolution of calcium carbonate crystals in pure water and  $MgSO_4$  solutions with different concentrations. Specifically, the term “RT-pure water” represents samples treated under conditions of pure water.

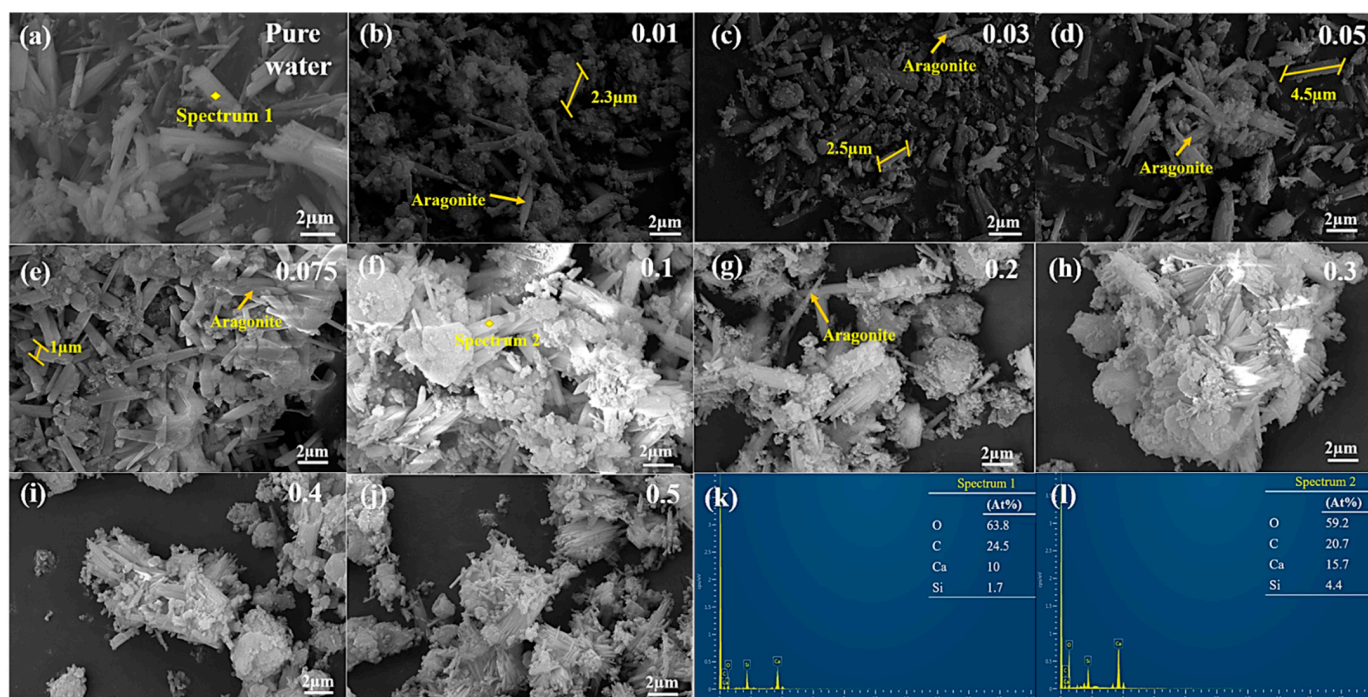


**Figure 8.** SEM image of MS carbonated with different  $MgSO_4$  concentrations ((a) 80 °C pure water, (b) 0.01 M, (c) 0.03 M, (d) 0.05 M, (e) 0.075 M, (f) 0.1 M, (g) 0.2 M, (h) 0.3 M, (i) 0.4 M, (j) 0.5 M, (k) EDS 1, (l) EDS 2).

From Figure 8, it can be observed that, under pure water conditions, the MS samples subjected to wet carbonation have generated a large number of aragonite crystals. However, these crystals exhibit a low aspect ratio, mostly taking on a short rod-like shape, and are surrounded by numerous calcite particles. In comparison, the aragonite crystals generated in the S-0.01 experimental group are noticeably longer and have smaller diameters.

As the concentration of  $MgSO_4$  increases, the quantity of aragonite crystals increases while the corresponding calcite particles decrease. It is only when the concentration reaches 0.075 M that a substantial number of long rod-like aragonite crystals with diameters smaller than 1  $\mu m$  are obtained. However, it appears that excessively high concentrations of  $MgSO_4$  have a negative impact on the growth of aragonite. When the concentration exceeds 0.1 M, aggregate phenomena are observed in the aragonite crystals, and many block-like particles adhere to the surface, with the aggregation becoming more pronounced as the concentration further increases. It is not until the  $MgSO_4$  concentration reaches 0.5 M that the block-like particles disappear, being replaced by numerous aragonite aggregates with diameters smaller than 0.5  $\mu m$ .

This phenomenon can be attributed to the addition of  $Mg^{2+}$ , which stabilizes the crystal structure of aragonite and inhibits the transformation of aragonite crystals into calcite [48]. Furthermore, an appropriate concentration of  $Mg^{2+}$  can also suppress rapid growth in the aragonite diameter, thereby enhancing the aspect ratio of the aragonite crystals. However, when the  $MgSO_4$  concentration becomes too high, a large amount of  $Mg^{2+}$  is added, leading to an increase in nucleation sites and subsequent aggregation

of aragonite crystals [34]. Additionally, excessive concentrations of  $\text{MgSO}_4$  introduce a significant amount of  $\text{SO}_4^{2-}$ , which reacts with the dissolved  $\text{Ca}^{2+}$  in the suspension to form dihydrate gypsum that adheres to the surface of aragonite crystals.

By comparing the microstructures of C-MS under different concentrations of  $\text{MgSO}_4$  solution, it can be concluded that the S-0.075 experimental group yields the highest quantity of long rod-like aragonite crystals with diameters smaller than  $1\ \mu\text{m}$ , and it exhibits the highest aspect ratio.

### 3.3. Effect of Aragonite Whisker on Cement Paste

#### 3.3.1. Compressive Strength

Figure 9 illustrates the influence of different C-MS contents (0–5%) on the compressive strength of cement paste. The C-MS was obtained under optimal conditions, i.e., 0.075 M  $\text{MgSO}_4$ .

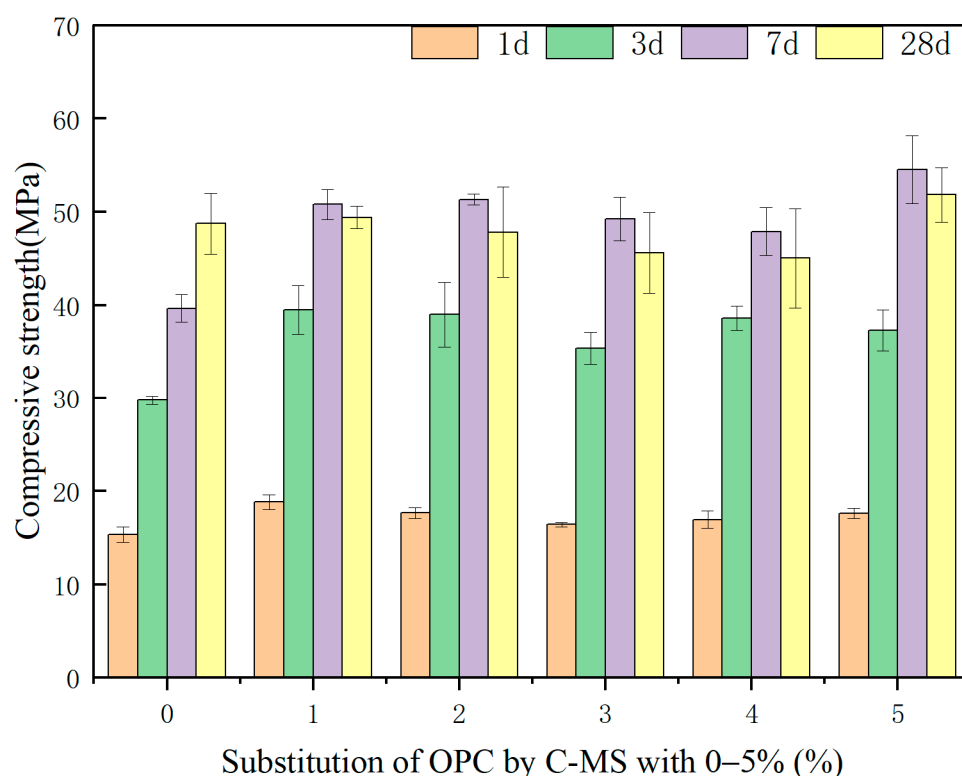


**Figure 9.** Effect of C-MS on the compressive strength of cement paste.

The results indicate that at a curing time of one day, the compressive strength of the experimental group is similar to the control group. At three and seven days, the compressive strength of the experimental group is generally higher than that of the control group. Particularly, at a substitution level of 5%, the compressive strength of the experimental group increases by 37.5% at seven days, reaching 54 MPa. This suggests that the addition of C-MS significantly enhances the early strength of cement paste, primarily due to the filling effect of carbonates and the accelerated hydration reaction of cement at early stages [55].

After a curing period of 28 days, the compressive strength of the experimental group shows a slight decrease. However, at a substitution level of 5%, the compressive strength of the cement paste is still significantly higher than that of the control group. This may be attributed to the carbonates accelerating the early hydration of cement paste, leading to a decrease in nucleation points of later hydration products or a weakening of the filling effect of carbonates, resulting in a slight decrease.

These results demonstrate that the preparation of aragonite whiskers using MS in conjunction with  $\text{MgSO}_4$  in wet carbonation can significantly improve the early mechanical

properties of cement paste. This not only enables the absorption of carbon dioxide and reduces cement consumption, thereby achieving low-carbon goals in the cement industry but also realizes the high-value reuse of MS.

### 3.3.2. Fracture Surface Micromorphology

Sampling was conducted on the natural fracture surface of cement specimens from the 28-day curing period of the 5% experimental group. The obtained samples were soaked in anhydrous ethanol for 24 h and then dried in a vacuum oven at 50 °C. SEM testing was performed to investigate the microstructure morphology, as shown in Figure 10.

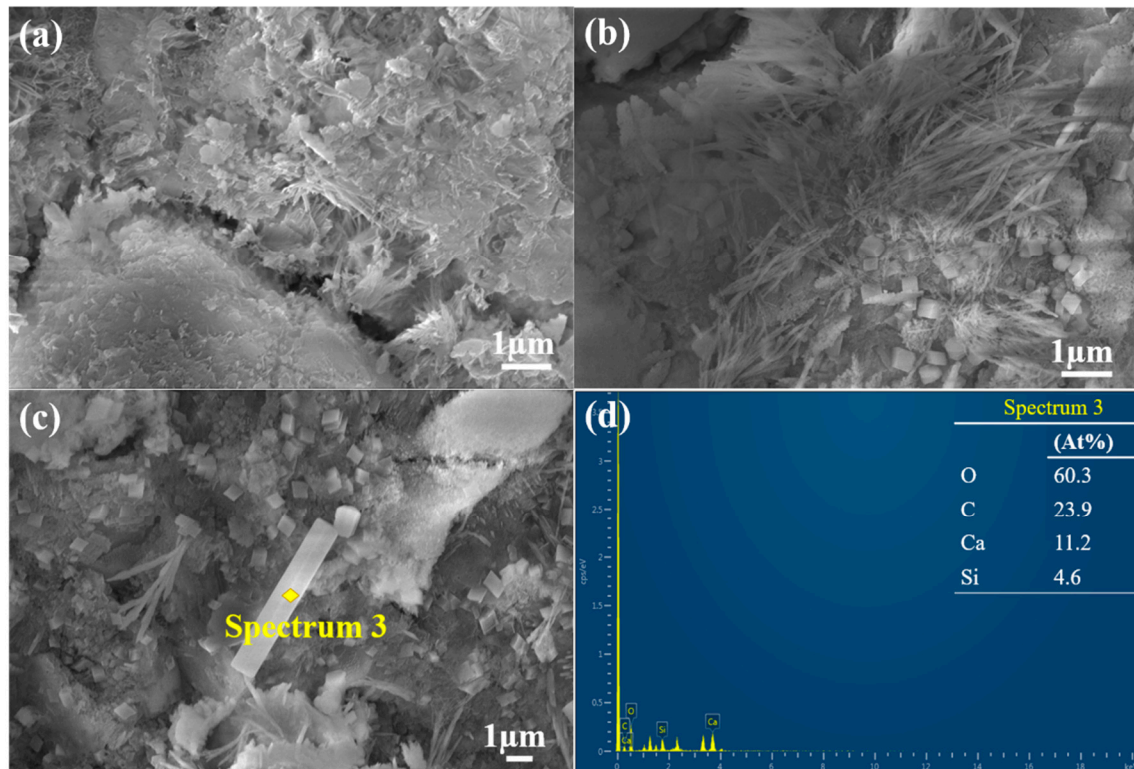


**Figure 10.** SEM images of cement paste fracture surfaces: (a) control; (b) 5% C-MS; (c) 5% C-MS; (d) EDS.

From the results, it can be observed that in the control group (a), the interior of the paste is relatively loose and porous, with needle-like ettringite present. This is due to the ongoing hydration reaction of silicate minerals within the specimen during the later stage of curing. In the 5% C-MS sample (b), not only is there a larger quantity of ettringite crystals, but also a significant amount of cubic calcite can be observed. These cubic calcite crystals densely aggregate within the paste, reducing the pore structure and resulting in a more compact cement matrix. This change in microstructure, along with the filling effect of calcium carbonate, significantly enhances the mechanical properties of the cement paste.

Additionally, in the experimental group (c), distinct rod-shaped aragonite can be observed, surrounded by numerous calcite crystals and hydration products. Based on the above results, it can be concluded that the improvement in compressive strength of the cement paste is attributed to the introduction of carbonates, which provide nucleation sites for the formation of hydrated products (C-S-H) and accelerate the hydration reaction of the cement paste, leading to an increase in hydration products [56–58]. Furthermore, the interaction between calcite and aragonite enhances the internal structure of the paste, reduces porosity through the filling effect, and further improves the compressive performance of the cement paste [59]. This is consistent with the compressive strength results.

### 3.4. CO<sub>2</sub> Sequestration

Based on the TG-DTG test results and in combination with Equations (1) and (2), the carbon dioxide (CO<sub>2</sub>) sequestration efficiency was calculated. It is important to note that in the actual calculation results, the CO<sub>2</sub> content in the raw materials before carbonation should be excluded.

$$\text{CO}_2 \text{ TG} = M_{500^\circ\text{C}} - M_{800^\circ\text{C}} \quad (1)$$

$$\text{CO}_2 \text{ content} = \text{CO}_2 \text{ TG} - \text{CO}_2 \text{ materials} \quad (2)$$

In this context, CO<sub>2</sub> TG represents the mass loss of the sample between 500 and 800 °C, and M<sub>500°C</sub> and M<sub>800°C</sub> represent the mass of the sample at 500 °C and 800 °C, respectively. CO<sub>2</sub> content represents the carbonation amount of the sample, and CO<sub>2</sub> materials represent the amount of CO<sub>2</sub> absorbed by the raw materials during transportation.

Through calculations, it was determined that the CO<sub>2</sub> sequestration efficiency of the S-0.075 experimental group reaches 19.62 g CO<sub>2</sub>/100 g MS. This calculation, combined with the compressive strength results, provides substantial evidence for the dual benefits of incorporating C-MS rich in calcite whiskers into cement. Not only does it enhance the physical properties of the cement paste, but it also effectively sequesters a significant amount of CO<sub>2</sub>, contributing to achieving carbon emission reduction targets in the cement industry.

## 4. Conclusions

In this study, magnesium sulfate (MgSO<sub>4</sub>) was selected as a calcium carbonate crystal modifier to selectively prepare aragonite whiskers. The aim was to investigate the influence of the joint action of SO<sub>4</sub><sup>2-</sup> and Mg<sup>2+</sup> on the crystal phase transformation of calcium carbonate, achieving high-value recovery and sequestration of CO<sub>2</sub> while enhancing cement performance. The following are the main conclusions drawn from this research:

1. The presence of Mg<sup>2+</sup> and SO<sub>4</sub><sup>2-</sup> simultaneously affects the phase composition of carbonation products. When the MgSO<sub>4</sub> concentration is less than 0.1 M, the carbonation products mainly consist of aragonite, calcite, gel, and amorphous calcium carbonate. The content of aragonite increases with increasing concentration. When the MgSO<sub>4</sub> concentration exceeds 0.1 M, calcite disappears, and a new phase, dihydrate gypsum, appears with its content increasing with higher concentration.
2. The presence of Mg<sup>2+</sup> and SO<sub>4</sub><sup>2-</sup> simultaneously affects the morphology and size of the formed calcite crystals. When the MgSO<sub>4</sub> concentration is less than 0.075 M, the formed calcite crystals appear as elongated rods. When the concentration exceeds 0.1 M, the size of calcite crystals increases while the diameter decreases, forming slender strips with aggregation phenomena.
3. Incorporating the optimal concentration (0.075 M) of C-MS at a substitution rate of 5% into OPC enhances the compressive strength of the cement paste by 37.5% compared to the control group at an early stage (seven days).
4. MS subjected to wet carbonation demonstrates excellent CO<sub>2</sub> sequestration capacity. The CO<sub>2</sub> sequestration efficiency of the S-0.075 experimental group reaches 19.62 g CO<sub>2</sub> per 100 g MS.

The above research findings reveal the importance of magnesium sulfate in regulating the crystal phase of calcium carbonate and enhancing cement performance, providing a new avenue for the efficient utilization of MS and CO<sub>2</sub> sequestration.

**Author Contributions:** Methodology, S.L.; Software, J.Y.; Validation, J.F.; Formal analysis, J.Y. and J.F.; Investigation, S.L. and X.G.; Data curation, J.Y.; Writing—original draft, J.Y.; Writing—review & editing, J.Y.; Supervision, S.L., J.F., H.Z. and J.Z.; Project administration, S.L.; Funding acquisition, S.L., J.F. and X.G. All authors have read and agreed to the published version of the manuscript.

**Funding:** This research was funded by the National Key R&D Program Intergovernmental International Science and Technology Innovation Cooperation Project (2018YFE0107300), the China Building

Materials Federation (20221JBGS03-11), the Science and Technology Project of Henan Province (211110231400, 212102310559, 212102310564, 222300420167, 22A430022), the Opening Project of the State Key Laboratory of Green Building Materials (2021GBM06), and the Henan Outstanding Foreign Scientists' Workroom (GZS2021003).

**Data Availability Statement:** The data used to support the findings of this research are available from the corresponding author upon request. The data are not publicly available due to privacy.

**Conflicts of Interest:** The authors declare no conflict of interest.

## References

1. Santos, R.L.; Horta, R.B.; Pereira, J.; Nunes, T.G.; Rocha, P.; Canongia Lopes, J.N.; Colaço, R. Microstructural control and hydration of novel micro-dendritic clinkers with  $\text{CaO}/\text{SiO}_2 = 1.4$ . *Cem. Concr. Res.* **2015**, *76*, 212–221. [[CrossRef](#)]
2. Shia, C.; Qua, B.; Provis, J.L. Recent progress in low-carbon binders. *Cem. Concr. Res.* **2019**, *122*, 227–250. [[CrossRef](#)]
3. Liao, Y.; Wang, S.; Wang, K.; Qunaynah, S.; Wan, S.; Yuan, Z.; Xu, P.; Tang, S. A study on the hydration of calcium aluminate cement pastes containing silica fume using non-contact electrical resistivity measurement. *J. Mater. Res. Technol.* **2023**, *24*, 8135–8149. [[CrossRef](#)]
4. Huang, J.; Li, W.; Huang, D.; Wang, L.; Chen, E.; Wu, C.; Wang, B.; Deng, H.; Tang, S.; Shi, Y.; et al. Fractal Analysis on Pore Structure and Hydration of Magnesium Oxysulfate Cements by First Principle, Thermodynamic and Microstructure-Based Methods. *Fractal Fract.* **2021**, *5*, 164. [[CrossRef](#)]
5. Li, Y.; Zhang, H.; Huang, M.; Yin, H.; Jiang, K.; Xiao, K.; Tang, S. Influence of Different Alkali Sulfates on the Shrinkage, Hydration, Pore Structure, Fractal Dimension and Microstructure of Low-Heat Portland Cement, Medium-Heat Portland Cement and Ordinary Portland Cement. *Fractal Fract.* **2021**, *5*, 79. [[CrossRef](#)]
6. Shen, W.; Cao, L.; Li, Q.; Zhang, W.; Wang, G.; Li, C. Quantifying CO<sub>2</sub> emissions from China's cement industry. *Renew. Sustain. Energy Rev.* **2015**, *50*, 1004–1012. [[CrossRef](#)]
7. Ashraf, W.; Olek, J. Carbonation activated binders from pure calcium silicates: Reaction kinetics and performance controlling factors. *Cem. Concr. Compos.* **2018**, *93*, 85–98. [[CrossRef](#)]
8. Liao, Y.; Yao, J.; Deng, F.; Li, H.; Wang, K.; Tang, S. Hydration behavior and strength development of supersulfated cement prepared by calcined phosphogypsum and slaked lime. *J. Build. Eng.* **2023**, *80*, 108075. [[CrossRef](#)]
9. Liao, Y.; Jiang, G.; Wang, K.; Al Qunaynah, S.; Yuan, W. Effect of steel slag on the hydration and strength development of calcium sulfoaluminate cement. *Constr. Build. Mater.* **2020**, *265*, 120301. [[CrossRef](#)]
10. Hasanbeigi, A.; Price, L.; Lin, E. Emerging energy-efficiency and CO<sub>2</sub> emission-reduction technologies for cement and concrete production: A technical review. *Renew. Sustain. Energy Rev.* **2012**, *16*, 6220–6238. [[CrossRef](#)]
11. Liu, S.; Rong, P.; Zhang, C.; Lu, J.; Guan, X.; Shi, C.; Zhu, J. Preparation and carbonation hardening of low calcium CO<sub>2</sub> sequestration materials from waste concrete powder and calcium carbide slag. *Cem. Concr. Compos.* **2023**, *141*, 105151. [[CrossRef](#)]
12. Panesar, D.K.; Mo, L. Properties of binary and ternary reactive MgO mortar blends subjected to CO<sub>2</sub> curing. *Cem. Concr. Compos.* **2013**, *38*, 40–49. [[CrossRef](#)]
13. Knight, K.A.; Cunningham, P.R.; Miller, S.A. Optimizing supplementary cementitious material replacement to minimize the environmental impacts of concrete. *Cem. Concr. Compos.* **2023**, *139*, 105049. [[CrossRef](#)]
14. Liu, S.; Shen, P.; Xuan, D.; Li, L.; Sojobi, A.; Zhan, B.; Poon, C. A comparison of liquid-solid and gas-solid accelerated carbonation for enhancement of recycled concrete aggregate. *Cem. Concr. Compos.* **2021**, *118*, 103988. [[CrossRef](#)]
15. Zhu, C.; Fang, Y.; Wei, H. Carbonation-cementation of recycled hardened cement paste powder. *Constr. Build. Mater.* **2018**, *192*, 224–232. [[CrossRef](#)]
16. Zhang, D.; Ghouleh, Z.; Shao, Y. Review on carbonation curing of cement-based materials. *J. CO<sub>2</sub> Util.* **2017**, *21*, 119–131. [[CrossRef](#)]
17. Jiang, K.; Ashworth, P.; Zhang, S.; Hu, G. Print media representations of carbon capture utilization and storage (CCUS) technology in China. *Renew. Sustain. Energy Rev.* **2022**, *155*, 111938. [[CrossRef](#)]
18. Liu, Z.; Van den Heede, P.; Zhang, C.; Shi, X.; Wang, L.; Li, J.; Yao, Y.; Lothenbach, B.; De Belie, N. Carbonation of blast furnace slag concrete at different CO<sub>2</sub> concentrations: Carbonation rate, phase assemblage, microstructure and thermodynamic modelling. *Cem. Concr. Res.* **2023**, *169*, 107161. [[CrossRef](#)]
19. Chang, J.; Wang, D.; Fang, Y. Effects of mineralogical changes in BOFS during carbonation on pH and Ca and Si leaching. *Constr. Build. Mater.* **2018**, *192*, 584–592. [[CrossRef](#)]
20. Humbert, P.S.; Castro-Gomes, J. CO<sub>2</sub> activated steel slag-based materials: A review. *J. Clean. Prod.* **2019**, *208*, 448–457. [[CrossRef](#)]
21. Shah, V.; Scrivener, K.; Bhattacharjee, B.; Bishnoi, S. Changes in microstructure characteristics of cement paste on carbonation. *Cem. Concr. Res.* **2018**, *109*, 184–197. [[CrossRef](#)]
22. Zajac, M.; Skibsted, J.; Skocek, J.; Durdzinski, P.; Bullerjahn, F.; Ben Haha, M. Phase assemblage and microstructure of cement paste subjected to enforced, wet carbonation. *Cem. Concr. Res.* **2020**, *130*, 105990. [[CrossRef](#)]
23. Liu, P.; Yu, Z.; Chen, Y. Carbonation depth model and carbonated acceleration rate of concrete under different environment. *Cem. Concr. Compos.* **2020**, *114*, 103736. [[CrossRef](#)]

24. Sevelsted, T.F.; Skibsted, J. Carbonation of C–S–H and C–A–S–H samples studied by  $^{13}\text{C}$ ,  $^{27}\text{Al}$  and  $^{29}\text{Si}$  MAS NMR spectroscopy. *Cem. Concr. Res.* **2015**, *71*, 56–65. [[CrossRef](#)]
25. Wang, D.; Fang, Y.; Zhang, Y.; Chang, J. Changes in mineral composition, growth of calcite crystal, and promotion of physico-chemical properties induced by carbonation of  $\beta\text{-C}_2\text{S}$ . *J. CO<sub>2</sub> Util.* **2019**, *34*, 149–162. [[CrossRef](#)]
26. Wu, F.; You, X.; Wang, M.; Liu, T.; Lu, B.; Hou, G.; Jiang, R.; Shi, C. Increasing flexural strength of CO<sub>2</sub> cured cement paste by CaCO<sub>3</sub> polymorph control. *Cem. Concr. Compos.* **2023**, *141*, 105128. [[CrossRef](#)]
27. Peng, L.; Shen, P.; Poon, C.; Zhao, Y.; Wang, F. Development of carbon capture coating to improve the durability of concrete structures. *Cem. Concr. Res.* **2023**, *168*, 107154. [[CrossRef](#)]
28. Ketrane, R.; Leleyter, L.; Baraud, F.; Jeannin, M.; Gil, O.; Saidani, B. Characterization of natural scale deposits formed in southern Algeria groundwater. Effect of its major ions on calcium carbonate precipitation. *Desalination* **2010**, *262*, 21–30. [[CrossRef](#)]
29. Reddy, M.M.; Wang, K.K. Crystallization of calcium carbonate in the presence of metal ions. *J. Cryst. Growth* **1980**, *50*, 470–480. [[CrossRef](#)]
30. Ren, D.; Feng, Q.; Bourrat, X. Effects of additives and templates on calcium carbonate mineralization in vitro. *Micron* **2011**, *42*, 228–245. [[CrossRef](#)] [[PubMed](#)]
31. Fang, X.; Xuan, D.; Zhan, B.; Li, W.; Poon, C. Characterization and optimization of a two-step carbonation process for valorization of recycled cement paste fine powder. *Constr. Build. Mater.* **2021**, *278*, 122343. [[CrossRef](#)]
32. Cizer, Ö.; Van Balen, K.; Elsen, J.; Van Gemert, D. Real-time investigation of reaction rate and mineral phase modifications of lime carbonation. *Constr. Build. Mater.* **2012**, *35*, 741–751. [[CrossRef](#)]
33. Xu, X.; Guo, H.; Cheng, X.; Li, M. The promotion of magnesium ions on aragonite precipitation in MICP process. *Constr. Build. Mater.* **2020**, *263*, 120057. [[CrossRef](#)]
34. Shen, P.; Jiang, Y.; Zhang, Y.; Liu, S.; Xuan, D.; Lu, J.; Zhang, S.; Poon, C. Production of aragonite whiskers by carbonation of fine recycled concrete wastes: An alternative pathway for efficient CO<sub>2</sub> sequestration. *Renew. Sustain. Energy Rev.* **2023**, *173*, 113079. [[CrossRef](#)]
35. You, X.; Hu, X.; Xiao, Z.; Saleh Bairq, Z.; Chen, W.; Shi, C. Thermodynamic modelling of CaCO<sub>3</sub> polymorphs during CO<sub>2</sub> sequestration by cement slurry with the addition of MgCl<sub>2</sub>. *J. Clean. Prod.* **2023**, *410*, 137294. [[CrossRef](#)]
36. Waly, T.; Waly, T.; Kennedy, M.; Witkamp, G.; Amy, G.; Schippers, J. The role of inorganic ions in the calcium carbonate scaling of seawater reverse osmosis systems. *Desalination* **2012**, *284*, 279–287. [[CrossRef](#)]
37. Ye, J.; Liu, S.; Zhao, Y.; Li, Y.; Fang, J.; Zhang, H.; Guan, X. Development of Ultrafine Mineral Admixture from Magnesium Slag and Sequestration of CO<sub>2</sub>. *Buildings* **2023**, *13*, 204. [[CrossRef](#)]
38. Xie, G.; Suo, Y.; Liu, L.; Zhu, M.; Xie, L.; Qu, H.; Sun, W. Mechanical grinding activation of modified magnesium slag and its use as backfilling cementitious material. *Case Stud. Constr. Mater.* **2023**, *18*, e01778. [[CrossRef](#)]
39. Ruan, S.; Liu, L.; Shao, C.; Xie, L.; Zhu, M.; Wang, R. Study on the source of activity and differences between modified and unmodified magnesium slag as a filling cementitious materials. *Constr. Build. Mater.* **2023**, *392*, 132019. [[CrossRef](#)]
40. Ruan, S.; Liu, L.; Zhu, M.; Shao, C.; Xie, L. Development and field application of a modified magnesium slag-based mine filling cementitious material. *J. Clean. Prod.* **2023**, *419*, 138269. [[CrossRef](#)]
41. Zhang, C.; Liu, S.; Tang, P.; Guan, X.; Shi, C. Enhancing the hardening properties and microstructure of magnesium slag blocks by carbonation-hydration sequential curing. *J. Build. Eng.* **2023**, *76*, 107414. [[CrossRef](#)]
42. Mo, L.; Panesar, D.K. Accelerated carbonation—A potential approach to sequester CO<sub>2</sub> in cement paste containing slag and reactive MgO. *Cem. Concr. Compos.* **2013**, *43*, 69–77. [[CrossRef](#)]
43. Mo, L.; Hao, Y.; Liu, Y.; Wang, F.; Deng, M. Preparation of calcium carbonate binders via CO<sub>2</sub> activation of magnesium slag. *Cem. Concr. Res.* **2019**, *121*, 81–90. [[CrossRef](#)]
44. Aryal, M.; Liakopoulou-Kyriakides, M. Equilibrium, kinetics and thermodynamic studies on phosphate biosorption from aqueous solutions by Fe(III)-treated *Staphylococcus xylosum* biomass: Common ion effect. *Colloids Surf. A Physicochem. Eng. Asp.* **2011**, *387*, 43–49. [[CrossRef](#)]
45. Hao, J.; Cheng, G.; Hu, T.; Guo, B.; Li, X. Preparation of high-performance building gypsum by calcining FGD gypsum adding CaO as crystal modifier. *Constr. Build. Mater.* **2021**, *306*, 124910. [[CrossRef](#)]
46. Wu, C.; He, J.; Wang, K.; Yang, L.; Wang, F. Enhance the mechanical and water resistance performance of flue gas desulfurization gypsum by quaternary phase. *Constr. Build. Mater.* **2023**, *387*, 131565. [[CrossRef](#)]
47. Chen, Q.; Ding, W.; Sun, H.; Peng, T. Synthesis of anhydrite from red gypsum and acidic wastewater treatment. *J. Clean. Prod.* **2021**, *278*, 124026. [[CrossRef](#)]
48. Shen, P.; Lu, J.; Zhang, Y.; Jiang, Y.; Zhang, S.; Poon, C. Preparation aragonite whisker-rich materials by wet carbonation of cement: Towards yielding micro-fiber reinforced cement and sequestering CO<sub>2</sub>. *Cem. Concr. Res.* **2022**, *159*, 106891. [[CrossRef](#)]
49. Zhan, B.J.; Xuan, D.; Poon, C.; Scrivener, K. Characterization of interfacial transition zone in concrete prepared with carbonated modeled recycled concrete aggregates. *Cem. Concr. Res.* **2020**, *136*, 106175. [[CrossRef](#)]
50. Lu, B.; Drissi, S.; Liu, J.; Hu, X.; Song, B.; Shi, C. Effect of temperature on CO<sub>2</sub> curing, compressive strength and microstructure of cement paste. *Cem. Concr. Res.* **2022**, *157*, 106827. [[CrossRef](#)]
51. Wang, X.; Ni, W.; Wei, X.; Zhang, S.; Li, J.; Hu, W. Promotion effects of gypsum on carbonation of aluminates in medium Al ladle furnace refining slag. *Constr. Build. Mater.* **2022**, *336*, 127567. [[CrossRef](#)]

52. Jian, S.; Yang, X.; Gao, W.; Li, B.; Gao, X.; Huang, W.; Tan, H.; Lei, Y. Study on performance and function mechanisms of whisker modified flue gas desulfurization (FGD) gypsum. *Constr. Build. Mater.* **2021**, *301*, 124341. [[CrossRef](#)]
53. Ma, F.; Chen, C.; Wang, Y. Mechanical behavior of calcium sulfate whisker-reinforced paraffin/gypsum composites. *Constr. Build. Mater.* **2021**, *305*, 124795. [[CrossRef](#)]
54. Ding, X.; Wei, B.; Deng, M.; Chen, H.; Shan, Z. Effect of protein peptides with different molecular weights on the setting and hydration process of gypsum. *Constr. Build. Mater.* **2022**, *318*, 126185. [[CrossRef](#)]
55. Li, L.; Cao, M.; Yin, H. Comparative roles between aragonite and calcite calcium carbonate whiskers in the hydration and strength of cement paste. *Cem. Concr. Compos.* **2019**, *104*, 103350. [[CrossRef](#)]
56. Zajac, M.; Skocek, J.; Durdzinski, P.; Bullerjahn, F.; Skibsted, J.; Ben Haha, M. Effect of carbonated cement paste on composite cement hydration and performance. *Cem. Concr. Res.* **2020**, *134*, 106090. [[CrossRef](#)]
57. Li, M.; Yang, Y.; Liu, M.; Guo, X.; Zhou, S. Hybrid effect of calcium carbonate whisker and carbon fiber on the mechanical properties and microstructure of oil well cement. *Constr. Build. Mater.* **2015**, *93*, 995–1002. [[CrossRef](#)]
58. Lu, B.; Shi, C.; Zhang, J.; Wang, J. Effects of carbonated hardened cement paste powder on hydration and microstructure of Portland cement. *Constr. Build. Mater.* **2018**, *186*, 699–708. [[CrossRef](#)]
59. Cao, M.; Zhang, C.; Lv, H.; Xu, L. Characterization of mechanical behavior and mechanism of calcium carbonate whisker-reinforced cement mortar. *Constr. Build. Mater.* **2014**, *66*, 89–97. [[CrossRef](#)]

**Disclaimer/Publisher’s Note:** The statements, opinions and data contained in all publications are solely those of the individual author(s) and contributor(s) and not of MDPI and/or the editor(s). MDPI and/or the editor(s) disclaim responsibility for any injury to people or property resulting from any ideas, methods, instructions or products referred to in the content.